Study of Periodic and Aperiodic DBR Characteristics and Tamm modes

6^{th} *Semester Report*

Submitted in fulfillment of the requirements of
P398 Report

By

Yogendra Singh
Roll No. 1711148

Under the supervision of:

Dr. Ritwick Das

National Institute of Science Education and Research, Bhubaneswar
July 2021

Abstract

Study of Periodic and Aperiodic DBR Characteristics and Tamm modes

by Yogendra Singh

The following work concerns itself with the study of Surface States in periodic stratified medium (Distributed Bragg Reflectors). The symmetry between the periodic potential in Condensed matter Physics and its optical analogue in terms of refractive indices is exploited to develop a theoretical framework. A python program is developed to study the properties of periodic and aperiodic DBR, Tamm plasmon excitation and behaviour of resonant wavelength on varying parameters such as incident angles, varying widths of the material slabs, for a range of wavelength of incident light for different polarisation. ...

Contents

List of Figures

List of Tables

Chapter 1

Introduction

Study of Surface States offer great experimental opportunity. The dielectric/metal interface is nowadays extensively studied and new experiments are being designed to dwell in the mysteries of Surface states. The symmetry between the periodic potential in Condensed Matter Physics and its optical analogue in terms of alternate layers of different refractive indices can be exploited to develop a theoretical framework in which computational modelling and subsequent experimentation can be done. For this purpose, DBR is used as the Photonic Crystal. DBR or Distributed Bragg Reflector is a periodic arrangement of layers of different refractive indices. This system is analogous to periodic potential in a crystal. Hence, one can use this analogy and obtain similar dispersion relations. The forbidden band of a crystal corresponds to the range of frequencies at which the reflectivity of DBR is very high. Thus, for application purposes, DBRs in which high reflectivity are required. Using Transfer Matrix method, one can program and simulate the experimental results. Thus, the theoretical framework for the same is presented in the following chapter.

1.1 Photonic Crystals

A photonic crystal is a periodic optical nanostructure that affects the motion of photons inmuch the same way that ionic lattices affect electrons in solids.
Photonic crystals are composed of periodic dielectric, metallo-dielectric—or even superconductor microstructures or nanostructures that affect electromagnetic wave propagation in the same way that the periodic potential in a semiconductor crystal affects electrons by defining allowed and forbidden electronic energy bands. Photonic crystals contain regularly repeating regions of high and low dielectric constant. Photons (behaving as waves) either propagate through this structure or not, depending on their wavelength. Wavelengths that propagate are called modes,

and groups of allowed modes form bands.

Photonic crystals can be fabricated for one, two, or three dimensions. One-dimensional photonic crystals can be made of layers deposited or stuck together.Two-dimensional ones can be made by photolithography, or by drilling holes in a suitable substrate. Fabrication methods for three-dimensional ones include drilling under different angles, stacking multiple 2-D layers on top of each other, direct laser writing, or, for example, instigating self-assembly of spheres in a matrix and dissolving the spheres.

The periodic arrangement of atoms in a crystal provides a potential (V(x)) characterized by spatial periodicity

$$V(x+a) = V(x)$$

where a is a constant vector for a given crystal. Corresponding to this translational symmetry, Noether's theorem assures existence of a conserved quantity, known as crystal momentum(k). The eigenstates of Hamiltonian for this potential has a special structure. According to Bloch-Floquet theorem, the solutions are of the form

$$\Psi_k(r) = \mu_k(r) exp(ik.r)$$

where $\mu_k(r+a) = \mu_k(r)$. Let's restrict our consideration to one-dimensional situation only. The periodicity in real space, renders the momentum space to be periodic. A period in the momentum space is known as Brillouin Zone. The spectrum of this potential is obtained by solving the Schrödinger equation for each wave vector k , and hence we obtain the band structure.
The dispersion relation ($E(= h\omega) and k$) the band structure reveals that some energy states are not allowed,and hence there is a gap between two energy bands known as band gap. When

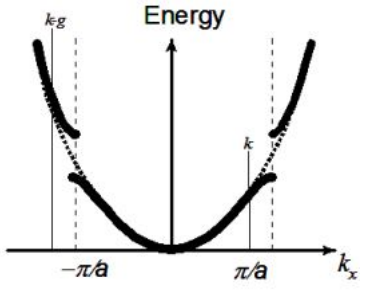

FIGURE 1.1

white light is incident on a stratified periodic structure, certain ranges of frequencies are reflected almost completely with reflectivity approaching unity. Due to this high reflectivity, these are also known as distributed Bragg Reflectors(DBR). Like the Schrödinger equation,

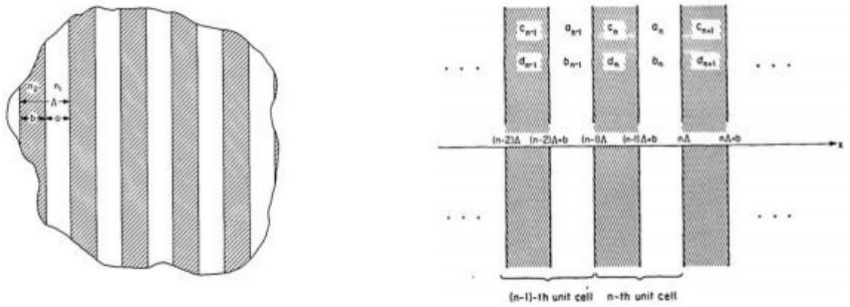

FIGURE 1.2

Maxwell's equations are also linear. Systems with no charge or current are known as sourceless. For the sourceless Ampere's and Faraday's law, an eigenvalue equation similar to that of Bloch Schrödinger equation is obtained. Akin to quantum mechanical Bloch States, the Bloch electromagnetic fields can be determined. Bloch -Floquet theorem applies, if there is a periodicity in the refractive index

$$n(x + a) = n(x)$$

The frequency ranges over which the reflectivity approaches unity corresponds to the bandgap of the dispersion relation obtained in this case. The translational symmetry of the refractive index in this situation is the reason of high reflectivity for certain frequency ranges. Abrupt change on this periodicity results in interesting phenomena.

1.2 Surface States

Once the symmetry is broken, the Bloch solution for periodic media gets modified. In particular, if the symmetry breaking occurs due to a layer of metal coated onto the surface of PhC, then a localized electric field of a particular wavelength in the photonic band gap is formed at the metal-PhC interface. These solutions decay exponentially along the normal to the crystal surface, hence they are localized at the surface and are called surface modes. Surface waves are those modes which propagate along the surface, while the ones which cannot, are known as surface states. Abrupt termination of periodic potential results in two kinds of solutions, depending on the kind of material used for periodic layers.

If the material is metallic or semiconducting, then we obtain the first kind of solutions, which are characterized by exponentially decaying continuation of the Bloch waves. On the other hand, if we use periodic dielectric layers act as a medium, we obtain second kind of solution, which has a localized maximum at the interface which decays exponentially on either side of it. In case of metal coated periodic stratified dielectric media, it is the localization of electromagnetic field at the metal-PhC interface which decays exponentially on either its side. This state is characterized

by a low reflectivity as well as low transmissivity at the Tamm wavelength. hence this state is non-propagating and is localized at the interface.

1.2.1 Tamm States

Particular surface states called optical Tamm states (OTSs) have attracted a lot of attention due to their huge potential for the fabrication of polariton lasers, optical data storage, and applications in analytical chemistry and medicine. Originally, Tamm states are electronic surface energies that are localized on crystal surfaces that were predicted by Tamm. Analogously, OTSs are surface modes that could be generated by perturbing properly periodic optical impedances at the surface of PhC. Unlike surface plasmon modes that are confined along the interface between a dielectric and a conductor, OTSs have a smaller wave vector in magnitude (parallel to the interface) compared with that of the light wave in vacuum. This enables a direct optical excitation of such modes for both transverse magnetic (TM) and transverse electric (TE) incident polarizations.

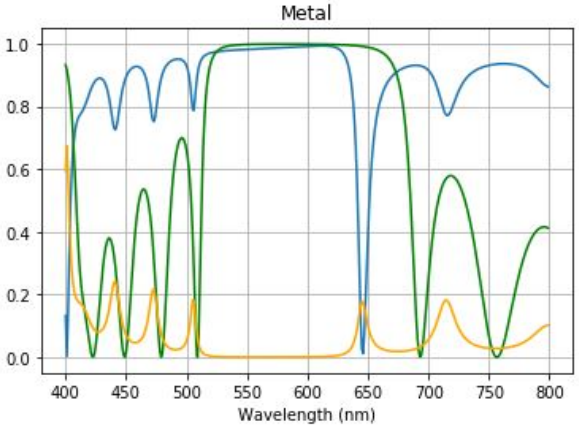

FIGURE 1.3: Just an example of DBR Spectra

Studying the reflectivity and transmittivity spectra, Tamm states in a metal-PhC can be identified. In the spectra given above, the green plot is that of reflectivity when no metal coating is there. The reflectivity (shown in blue color) increases as expected when metal is coated, but at 636 nm, in the photonic band gap, dip in reflectivity is observed. At this wavelength the transmissivity(in orange colour) is almost vanishing. To add to the confirmation of low values of reflectivity and transmissivity, we note that the absorption plot peaks at this particular wavelength. This allows us to infer that particular state has a localized field distribution inside the metal-PhC system. Thus the state at 636 nm is identified as a Tamm state. Field intensity distribution at this wavelength is localized at the interface of the metal and PhC.

1.3 Coventions and Setup

To determine the exact electromagnetic field we need the boundary conditions along with Maxwell's equations. For electromagnetic waves traveling from one medium to another separated by an infinite plane Maxwell's equationsalong with the boundary conditions reduce to Fresnel equations. Polarisation refers to the orientation of the electromagnetic field with respect to the infinite planar interface.
Consider an infinite planar interface passing through the origin and normal to $\widehat{x}$ We assume uniformity in the yz plane. The material on negative x-axis is of refractive index n_1, while that in the positive x-axis is n_2. The wavevector (k) of light is in the xy-plane, with the x-component of **k** being positive.
So the angle of incidence is θ_i, where

$$cos\theta_i = -\widehat{k}.\widehat{x}$$

The wavevector depends on the refractive index of the medium in which it is propagating. The magnitude of wavevector of light with angular frequency ω when it propagates through a medium of refractive index n is $k = n\omega/c$, where c is the speed of light in vacuum.
Let light be incident on the interface with angle of incidence θ_i. The component of wavevector perpendicular to the interface is $kcos\theta_i$, and that parallel to it is $ksin\theta_i = (n1\omega/c)sin\theta_i$. Snell's law ensures the parallel component being constant as light passes from the first medium to the second one

$$n_1 sin\theta_i = n_2 sin\theta_t$$

The electric field(**E**) and magnetic field(**H**) are perpendicular to the wavevector **k**. If the electromagnetic field is so oriented that the electric field is parallel to the planar interface then it is known as **s** polarisation. In this case, the magnetic field lies in the plane of incidence. On the other hand, if the magnetic field is parallel to the planar interface then it is known as **p** polarisation. In this case, the electric field is in the plane of incidence. The **E**-field component being parallel to the interface, in case of s-polarisation, is continuous across the sourceless media. For the case of p-polarisation, the same is true for **H**-field.
The coefficient of reflection is the ratio of reflected electric field amplitude to the incident field amplitude. Similarly, coefficient of transmission is defined as the ratio between the transmitted field amplitude to that of incident one. For light going from medium 1 to medium 2 we have

$$r_s = \frac{n_1 cos\theta_1 - n_2 cos\theta_2}{n_1 cos\theta_1 + n_2 cos\theta_2}$$

$$t_s = \frac{2n_1 cos\theta_1}{n_1 cos\theta_1 + n_2 cos\theta_2}$$

$$r_p = \frac{n_2 cos\theta_1 - n_1 cos\theta_2}{n_2 cos\theta_1 + n_1 cos\theta_2}$$

$$t_p = \frac{2n_1 cos\theta_1}{n_2 cos\theta_1 + n_1 cos\theta_2}$$

For a general periodic stratified medium, the wave amplitudes of neighbouring layers are related via the coefficients of reflection and transmission. We thus obtain a two-dimensional square matrix relating the amplitudes of electric field in the two medium. For multiple interfaces the wave amplitude on the either side of the layered material is are related by the product of matrices for each interface. Thus we obtain the reflectivity and transmissivity of the stratified medium. This method to compute the reflection and transmission coefficients is known as transfer matrix method. We have used this method in our computation.

Chapter 2

Computational Modelling

The theoretical framework for Surface States can be realised using the computational power to get the reflectivity and transmittance of a Distributed Bragg's Reflector (DBR). Hence, a Python Program was developed to simulate the quantities of interest like reflectivity spectra, transmittance spectra and the corresponding phase difference. Using such program, one can tweak different parameters and study their occurrence in actual experiments.
Although the general treatment for the phenomena is presented in the theoretical framework section, here, the computational technique used to develop the program is briefly discussed.

2.1 Computing the Reflectance and Transmittance Spectrum

For light going from medium 1 to medium 2, the reflection and transmission coefficient are obtained by theory. One can extend this argument for an interface where light can come from both the sides.
Let the amplitude at the interface are given as E_{f1}, E_{f2}, E_{b1} and E_{b2} where following notation convention is used:

- Latin subscript f : Amplitute of forward travelling wave
- Latin subscript, b : Amplitude of backward travelling wave
- Numerical subscript : The medium of propagation

These fields are related by the coefficients of reflection and transmission as :

$$E_{b1} = E_{f1} r_{12} + E_{b2} f_{21}$$

$$E_{f2} = E_{f1}t_{12} + E_{b2}r_{21}$$

where t_{12}, r_{12} are the respective coefficients for going from medium 1 to medium 2.
Now, consider a scenario where N interfaces are present and they are labelled from 0 to N-1. The forward and backward going wave amplitude between two adjacent layer are related by a two dimensional matrix. Let v_n and w_n are the forward and backward going wave amplitudes for the n^{th} interface. They are related to that of $(n-1)^{th}$ layer as

$$\begin{bmatrix} v_n \\ w_n \end{bmatrix} = M_n \begin{bmatrix} v_{n+1} \\ w_{n+1} \end{bmatrix}$$

for n = 1, 2, . . . N-2, where

$$M_n = \begin{bmatrix} e^{-i\delta_n} & 0 \\ 0 & e^{i\delta_n} \end{bmatrix} \begin{bmatrix} 1 & r_{n,n+1} \\ r_{n,n+1} & 1 \end{bmatrix} \frac{1}{t_{n,n+1}}$$

In order to determine the relative amplitudes of reflected and transmitted waves from a DBR, the incident amplitude is taken to be unity, the reflected amplitude would be r and the transmitted amplitude would be t. Thus

$$\begin{bmatrix} 1 \\ r \end{bmatrix} = M \begin{bmatrix} t \\ 0 \end{bmatrix}$$

where $M = \frac{1}{t_{0,1}} \begin{bmatrix} 1 & r_{0,1} \\ r_{0,1} & 1 \end{bmatrix} M_1 M_2 .... M_{N-1}$
Finally, the coefficient of reflectivity and transmittivity, (r and t) are obtained in terms of the matrix elements:

$$t = \frac{1}{M_{00}}$$

$$r = \frac{M_{10}}{M_{00}}$$

Taking the square of magnitude of r and t gives reflectivity (R) and transmittivity (T). This formalism is governed by the fact that for a given wavelength and incident angle, coefficient of reflection and transmission are unique.

2.2 Debugging unphysical cases for complex Refractive Indices

Whenever the Refractive index takes complex values, the incident angle for the corresponding medium also becomes complex. Due to this, the reflectivity comes to be greater than unity. Snell's law requires :

$$n_0 sin\theta_0 = n_i sin\theta_i$$

The value of $nsin\theta$ is real for every layer. Hence,

$$\theta = sin^{-}\left(\frac{n_i}{n_0} sin\theta_i\right)$$

Thus, θ as well as $\pi - \theta$ solves the equation. Hence, choice of theta is crucial and is efficiently handled by the program.

2.3 Metal Coating

The refractive index of metal is given by the Lorentz-Drude Model. For Gold, the relevant parameters are collision wavelength (8935.20 nm) and Plasma wavelength (168.26 nm). Using these, one can calculate the refractive index as

$$n^2 = 1 - \frac{\omega_p^2}{\omega^2 - i\omega_c\omega}$$

where ω,ω_p and ω_c are the angular frequency of incident light, plasma and collision angular frequency respectively.

Chapter 3

DBR Spectrum Computation and Observations

Different combinations of the widths of the cells of different refractive index media is considered to create different types of theoretical Distributed Bragg Reflectors(DBRs). Then the changes in the behaviour of Tamm modes of the most asymmetric DBR were studied under the change of incident angles for different polarisation and compared to the Tamm modes of a DBR with symmetric cells.
In a symmetric DBR with a metal coating in front, there is only one Tamm mode observed in one band gap, however in the asymmetric DBR, many Tamm modes are observed in band gaps.

3.1 Symmetric DBR

Here, we consider a DBR of 20 cells with width of a = 200 nm with refractive index $n_1 = 2.5$ and b = 200nm with refractive index $n_2 = 1.5$, with metal coating of Gold(Au) of width 35 nm and is studied in a range of wavelngth 400 nm - 2000 nm.

3.1.1 Angle Variation

Angle of incidence is varied from 0 to 90 degrees in the interval of 10 degrees and the behaviour of is observed.
The following are Reflectance(R) and Transmittance(T) vs wavelength graphs at different incident angles.

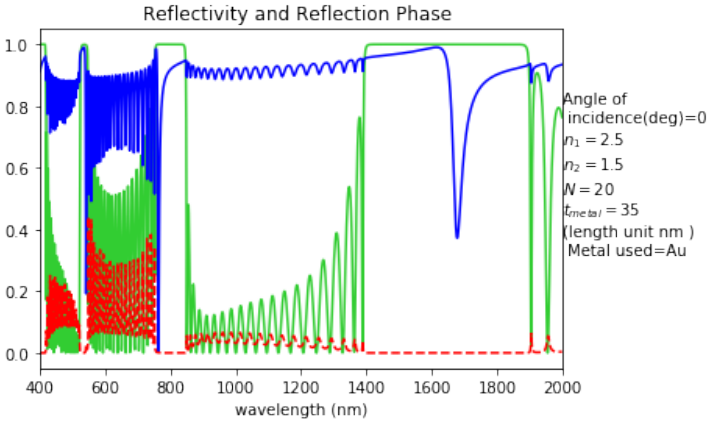

FIGURE 3.1: Symmetric DBR 0 degree

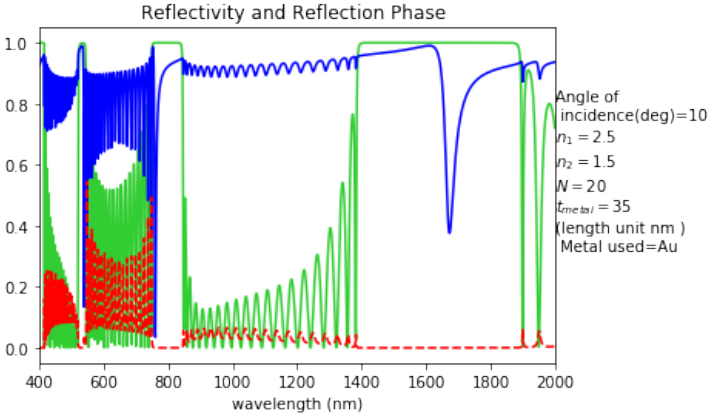

FIGURE 3.2: Symmetric DBR 10 degree

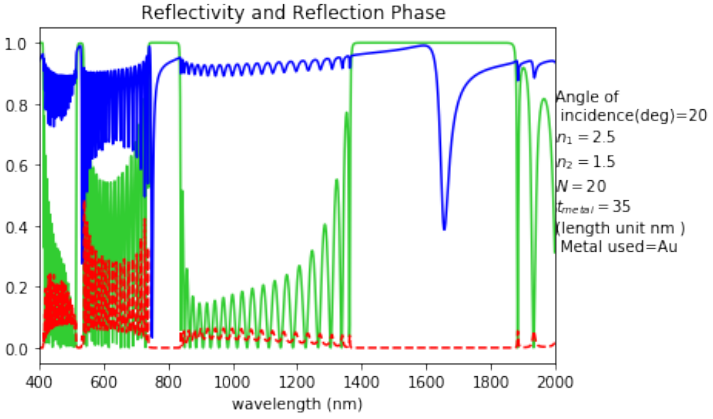

FIGURE 3.3: Symmetric DBR 20 degree

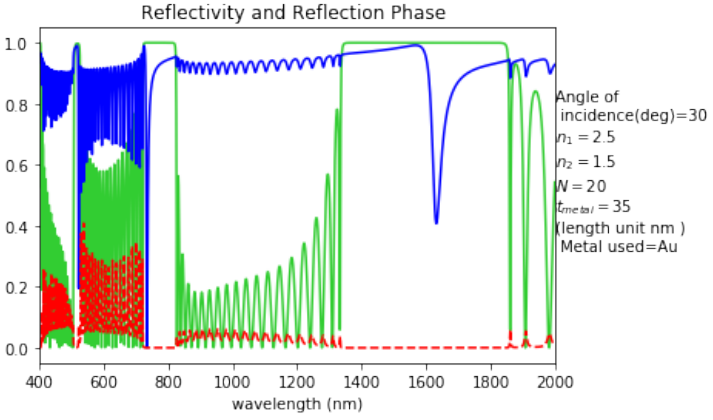

FIGURE 3.4: Symmetric DBR 30 degree

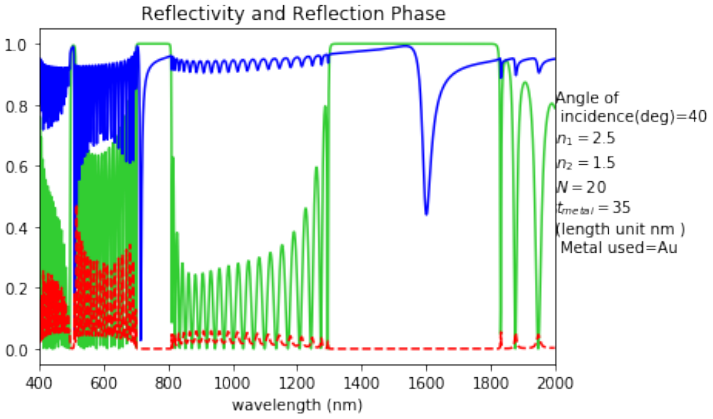

FIGURE 3.5: Symmetric DBR 40 degree

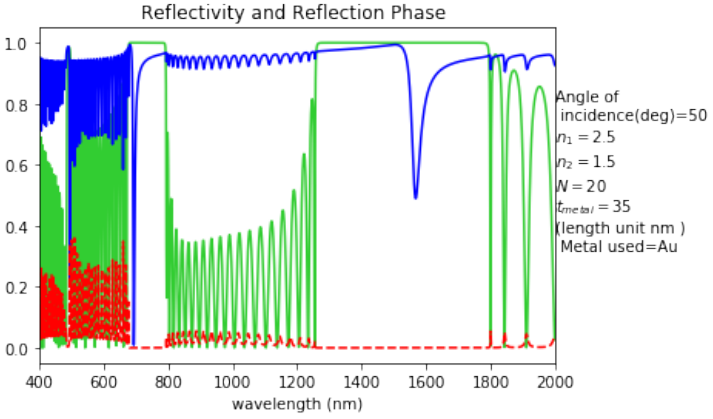

FIGURE 3.6: Symmetric DBR 50 degree

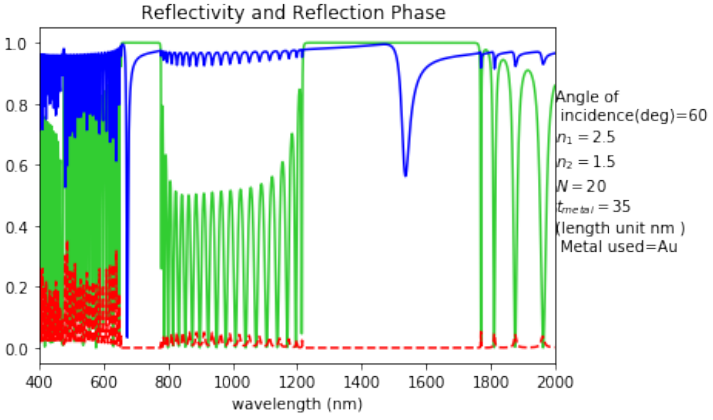

FIGURE 3.7: Symmetric DBR 60 degree

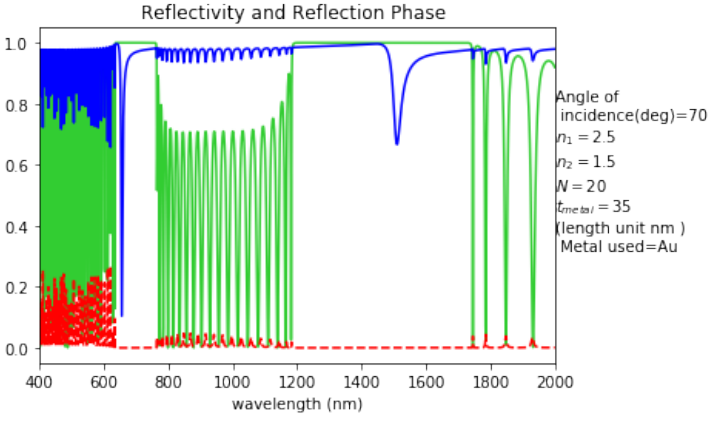

FIGURE 3.8: Symmetric DBR 70 degree

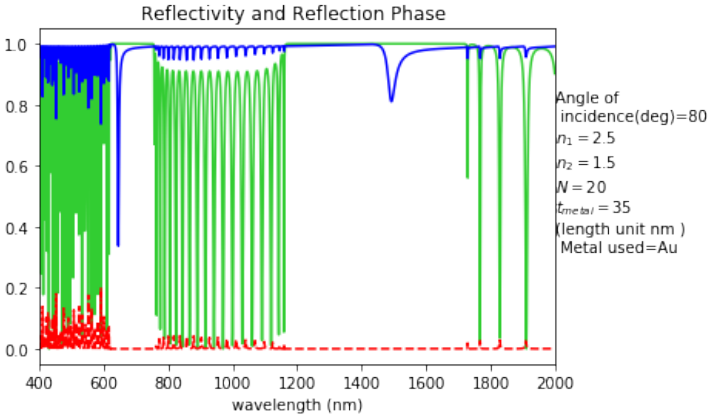

FIGURE 3.9: Symmetric DBR 80 degree

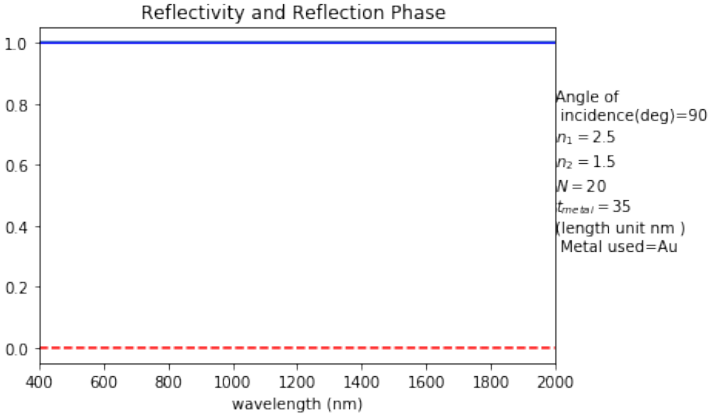

FIGURE 3.10: Symmetric DBR 90 degree

All of the above graphs are plotted for s polarisation.

3.1.2 Electric field Intensity

The electric field intensity is observed at the Tamm wavelength in the following graph:

.

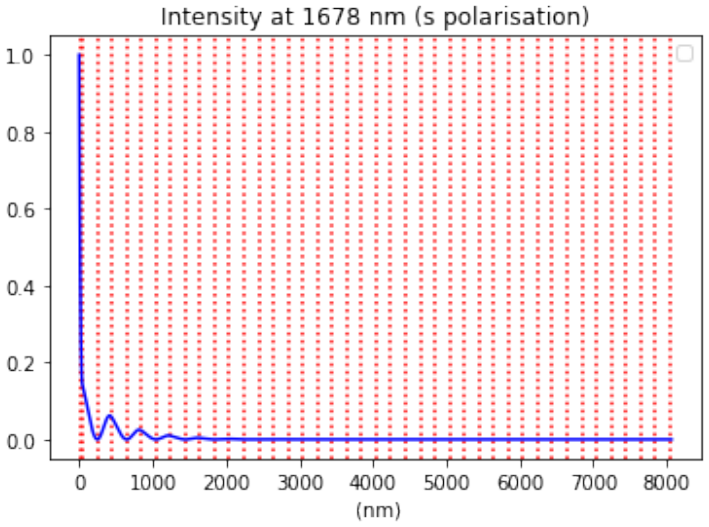

FIGURE 3.11: Electric field Intensity at 1678nm with 0 degree Incident angle

3.1.3 Effect on Tamm of s and p polarised light by angle variation

Tamm wavelength was measured for both s and p polarised light for different incident angles and the values obtained are as follows:

.

TABLE 3.1: Tamm of s and p polarised light variation

Incident Angle (in degrees)	s Tamm (nm)	p Tamm (nm)
0	1678	1678
15	1666	1664
30	1632	1624
45	1584	1565
60	1536	1499
75	1500	1446

These values of Tamm wavelengths are plotted against the angles and hence it is observed that the Tamm of s and p polarised light diverges from each other as the angle of incidence increases:

.

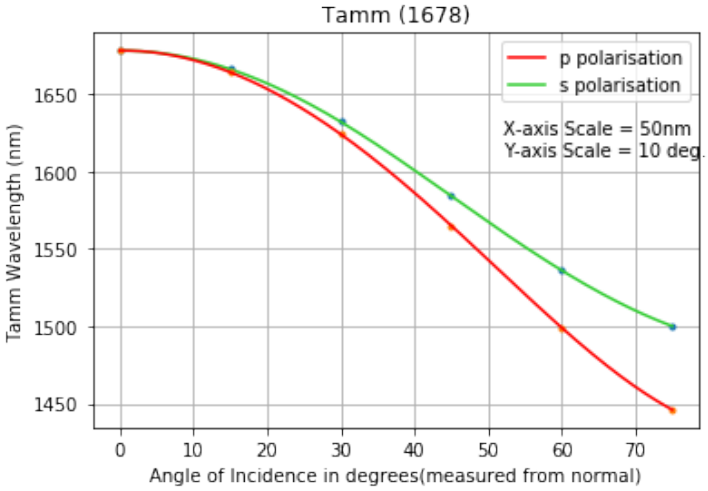

FIGURE 3.12: s and p Tamm wavelength vs Angle of Incidence

3.2 Asymmetric DBR

Here, we consider an asymmetric DBR of 39 cells with starting width of a = 10 nm with refractive index $n_1 = 2.5$ and b = 390nm with refractive index $n_2 = 1.5$, and with each succesive cell, the width of a increases 10nm and that of b decreases 10nm. The DBR has metal coating of Gold(Au) of width 35 nm at front and is studied in a range of wavelngth 400 nm - 2000 nm.

3.2.1 Angle Variation

Angle of incidence is varied from 0 to 90 degrees in the interval of 10 degrees and the behaviour of is observed.
The following are Reflectance(R) and Transmittance(T) vs wavelength graphs at different incident angles.

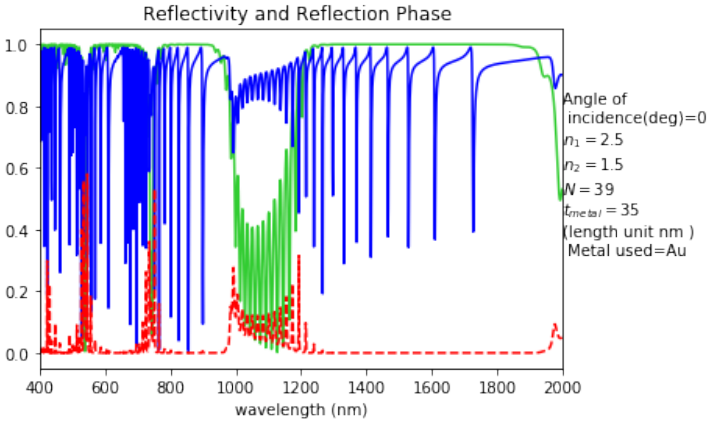

FIGURE 3.13: Asymmetric DBR 0 degree

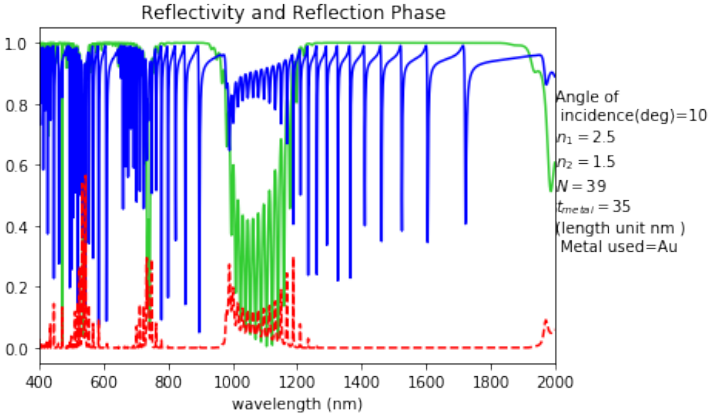

FIGURE 3.14: Asymmetric DBR 10 degree

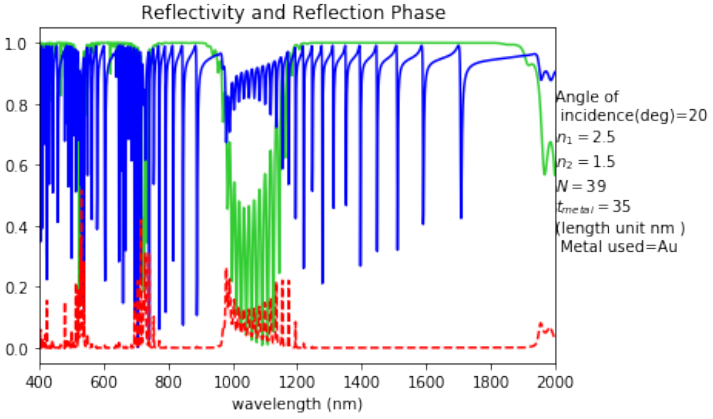

FIGURE 3.15: Asymmetric DBR 20 degree

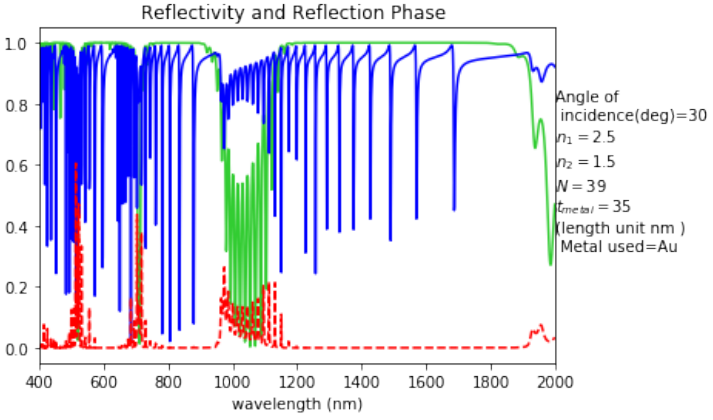

FIGURE 3.16: Asymmetric DBR 30 degree

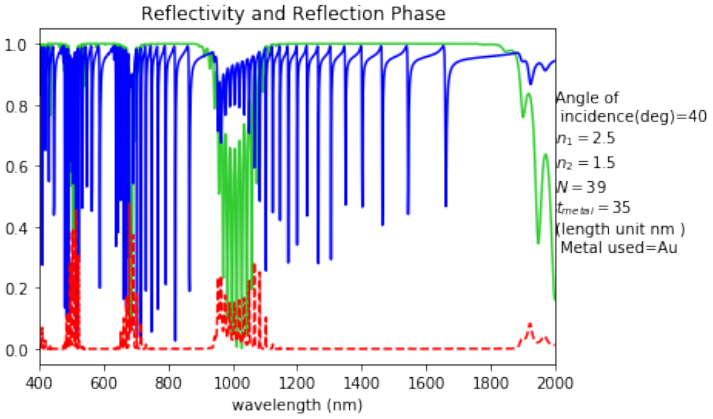

FIGURE 3.17: Asymmetric DBR 40 degree

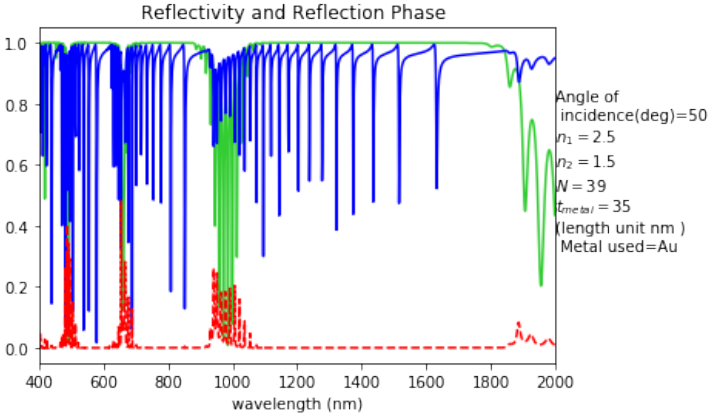

FIGURE 3.18: Asymmetric DBR 50 degree

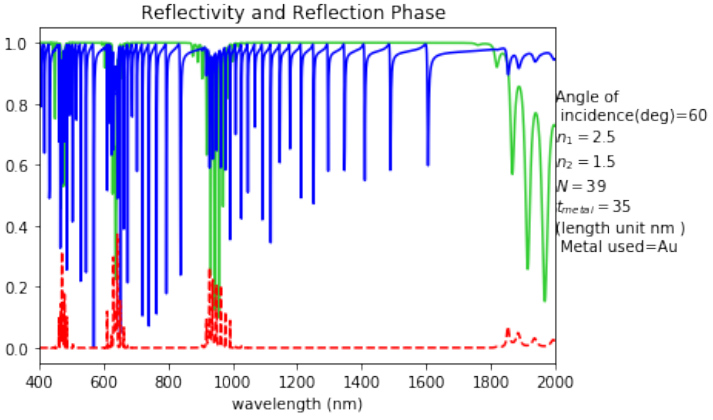

FIGURE 3.19: Asymmetric DBR 60 degree

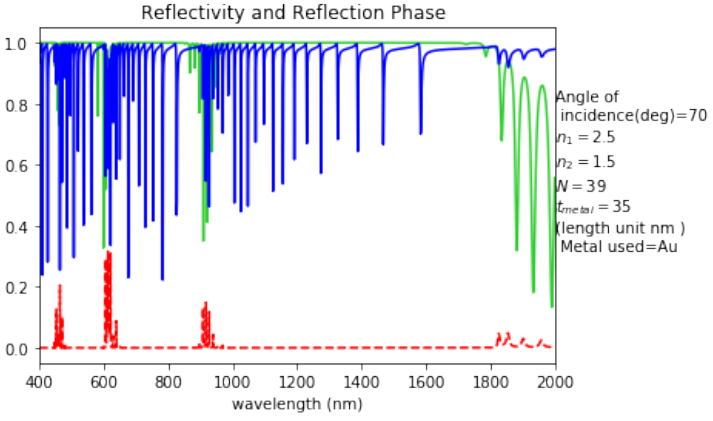

FIGURE 3.20: Asymmetric DBR 70 degree

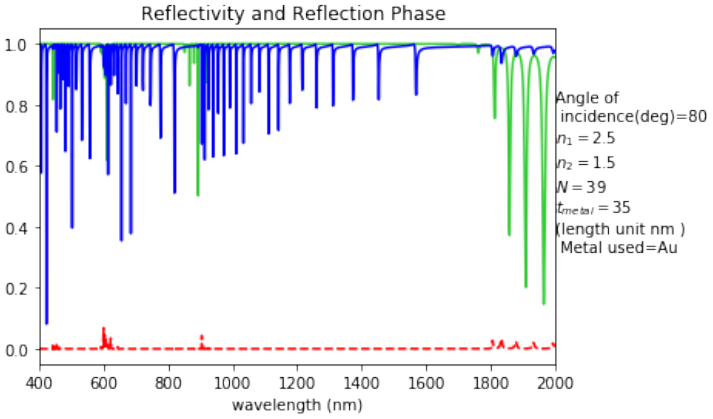

FIGURE 3.21: Asymmetric DBR 80 degree

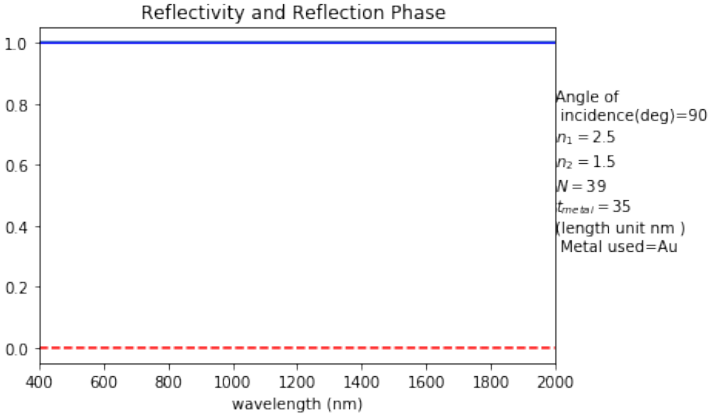

FIGURE 3.22: Asymmetric DBR 90 degree

3.2.2 Electric Field Intensity

The Electric field Intensity is observed for different Tamm wavelengths inside the band gap and is plotted against the distance x which ranges from the starting point of DBR to the end of it. The plots are made for 11 different Tamms:

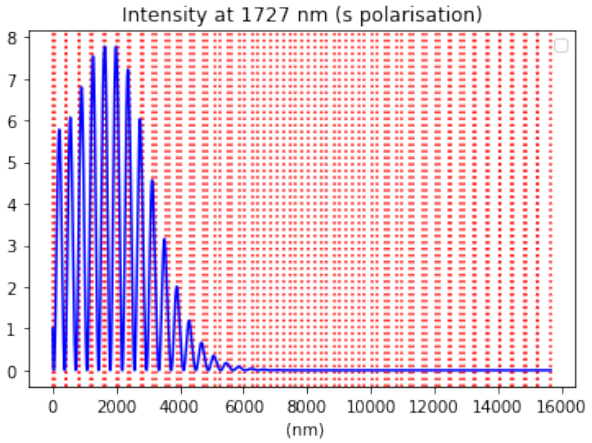

FIGURE 3.23: Intensity Profiling 1

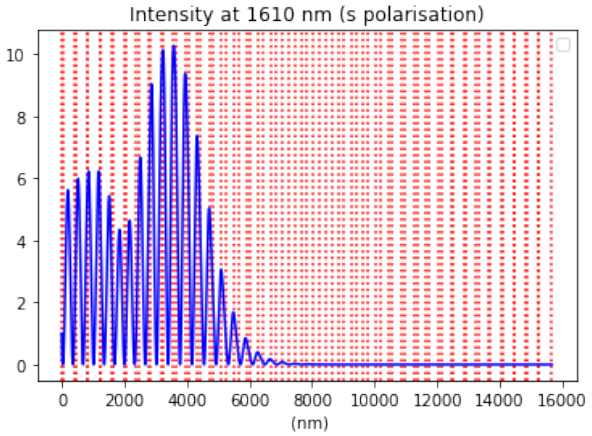

FIGURE 3.24: Intensity Profiling 2

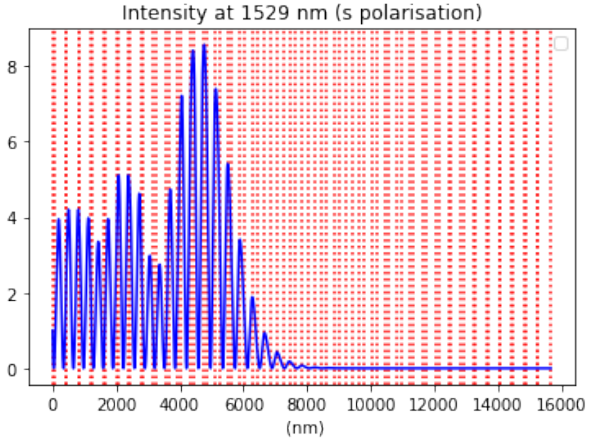

FIGURE 3.25: Intensity Profiling 3

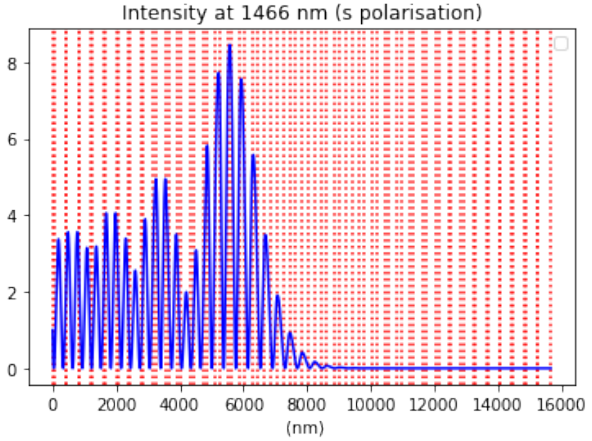

FIGURE 3.26: Intensity Profiling 4

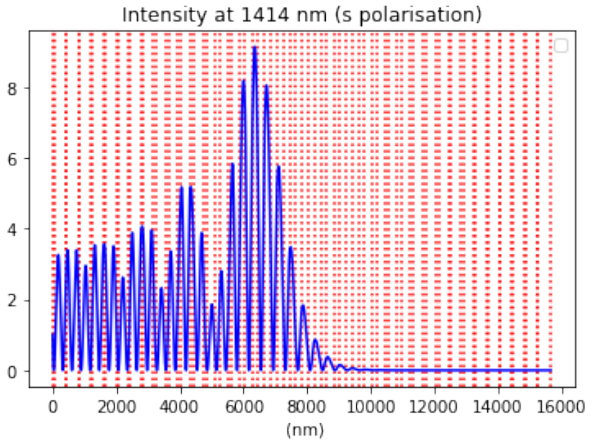

FIGURE 3.27: Intensity Profiling 5

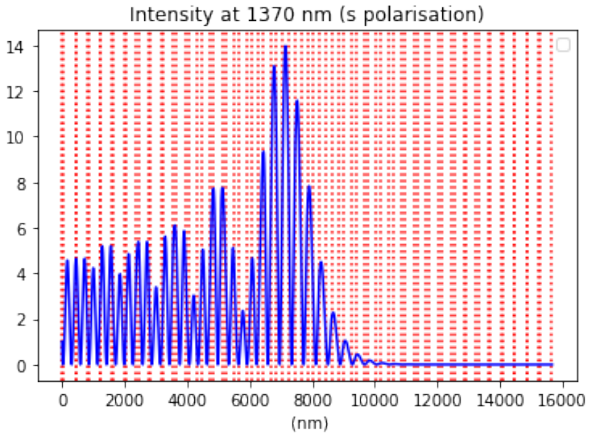

FIGURE 3.28: Intensity Profiling 6

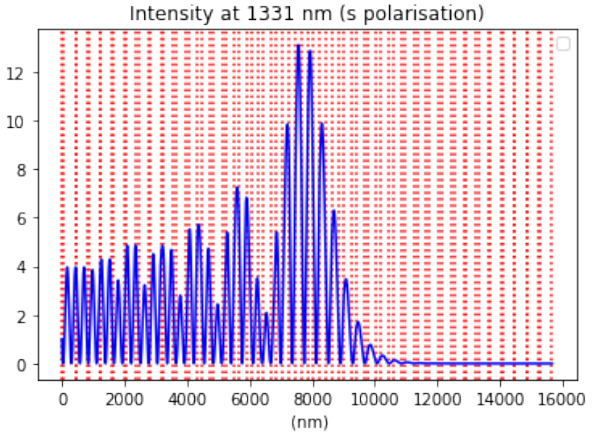

FIGURE 3.29: Intensity Profiling 7

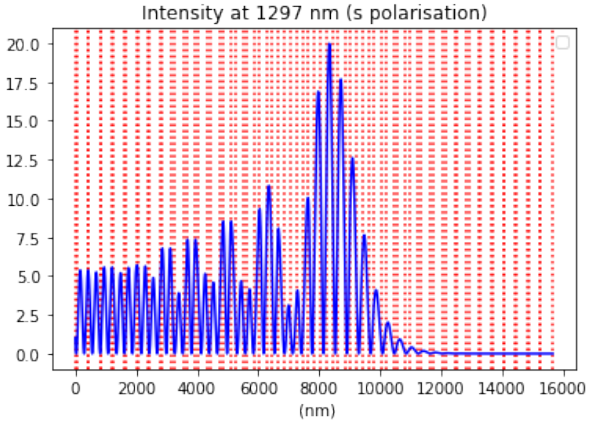

FIGURE 3.30: Intensity Profiling 8

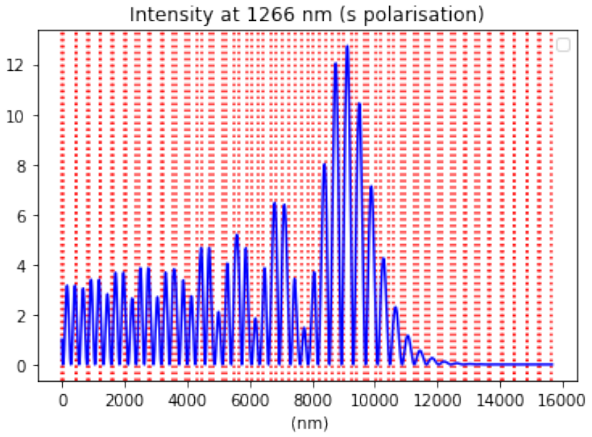

FIGURE 3.31: Intensity Profiling 9

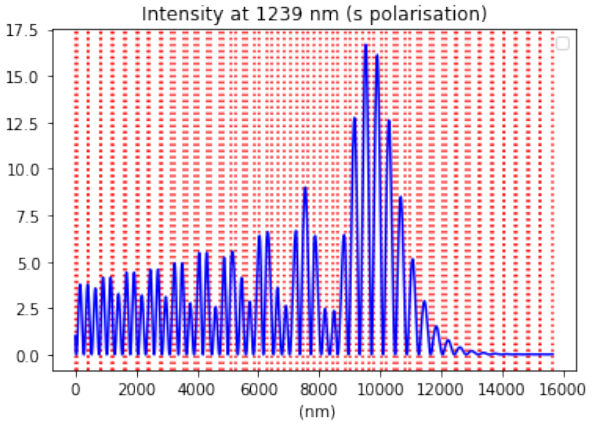

FIGURE 3.32: Intensity Profiling 10

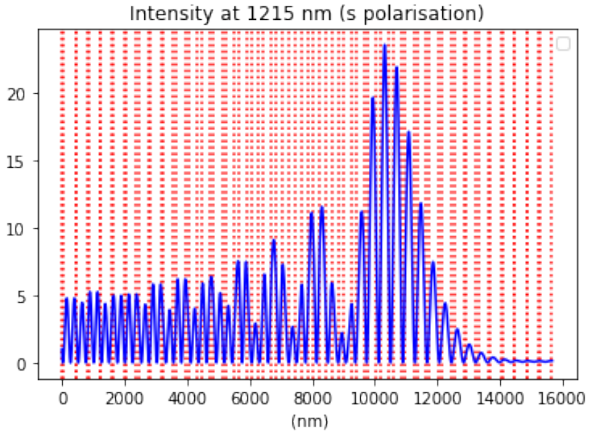

FIGURE 3.33: Intensity Profiling 11

3.2.3 Effect on Tamm of s and p polarised light by angle variation

All 11 Tamm wavelengths were measured for both s and p polarised light for different incident angles and the values obtained for each of them are as follows:

TABLE 3.2: s and p polarised Tamm variation 1

Incident Angle (in degrees)	s Tamm (nm)	p Tamm (nm)
0	1727	1727
15	1717	1717
30	1687	1691
45	1647	1653
60	1606	1613
75	1575	1583

TABLE 3.3: s and p polarised Tamm variation 2

Incident Angle (in degrees)	s Tamm (nm)	p Tamm (nm)
0	1610	1610
15	1599	1600
30	1570	1574
45	1530	1537
60	1489	1499
75	1459	1469

TABLE 3.4: s and p polarised Tamm variation 3

Incident Angle (in degrees)	s Tamm (nm)	p Tamm (nm)
0	1529	1529
15	1519	1520
30	1490	1494
45	1450	1458
60	1410	1420
75	1380	1391

.

TABLE 3.5: s and p polarised Tamm variation 4

Incident Angle (in degrees)	s Tamm (nm)	p Tamm (nm)
0	1466	1466
15	1456	1457
30	1428	1432
45	1388	1396
60	1347	1358
75	1317	1330

TABLE 3.6: s and p polarised Tamm variation 5

Incident Angle (in degrees)	s Tamm (nm)	p Tamm (nm)
0	1414	1414
15	1404	1405
30	1375	1380
45	1336	1344
60	1296	1307
75	1266	1279

TABLE 3.7: s and p polarised Tamm variation 6

Incident Angle (in degrees)	s Tamm (nm)	p Tamm (nm)
0	1370	1370
15	1359	1361
30	1331	1336
45	1291	1300
60	1251	1263
75	1222	1235

TABLE 3.8: s and p polarised Tamm variation 7

Incident Angle (in degrees)	s Tamm (nm)	p Tamm (nm)
0	1331	1331
15	1320	1322
30	1292	1297
45	1252	1262
60	1212	1225
75	1183	1197

TABLE 3.9: s and p polarised Tamm variation 8

Incident Angle (in degrees)	s Tamm (nm)	p Tamm (nm)
0	1297	1297
15	1286	1288
30	1257	1263
45	1218	1227
60	1178	1190
75	1148	1162

TABLE 3.10: s and p polarised Tamm variation 9

Incident Angle (in degrees)	s Tamm (nm)	p Tamm (nm)
0	1266	1266
15	1255	1257
30	1226	1232
45	1186	1196
60	1146	1159
75	1117	1131

TABLE 3.11: s and p polarised Tamm variation 10

Incident Angle (in degrees)	s Tamm (nm)	p Tamm (nm)
0	1239	1239
15	1228	1230
30	1199	1204
45	1158	1168
60	1118	1131
75	1089	1103

TABLE 3.12: s and p polarised Tamm variation 11

Incident Angle (in degrees)	s Tamm (nm)	p Tamm (nm)
0	1215	1215
15	1204	1205
30	1174	1179
45	1133	1143
60	1092	1105
75	1063	1077

3.2.4 Plots of s and p polarised Tamm with different angles

These values of Tamm wavelengths are plotted against the angles and hence it is observed that the Tamm of s and p polarised light diverges from each other as the angle of incidence increases:

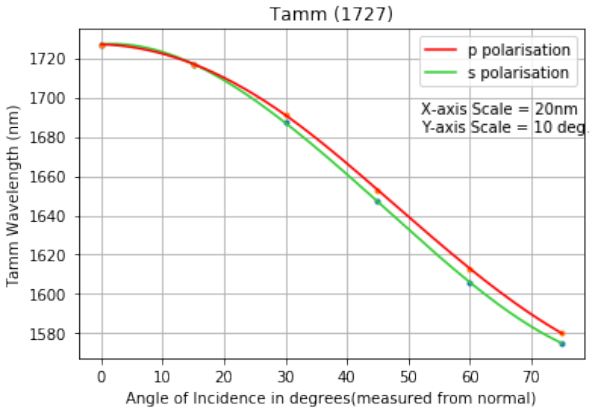

FIGURE 3.34: s and p Tamm wavelength vs Angle of Incidence 1

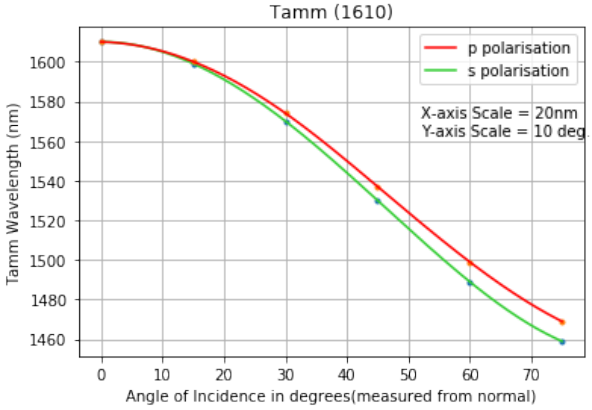

FIGURE 3.35: s and p Tamm wavelength vs Angle of Incidence 2

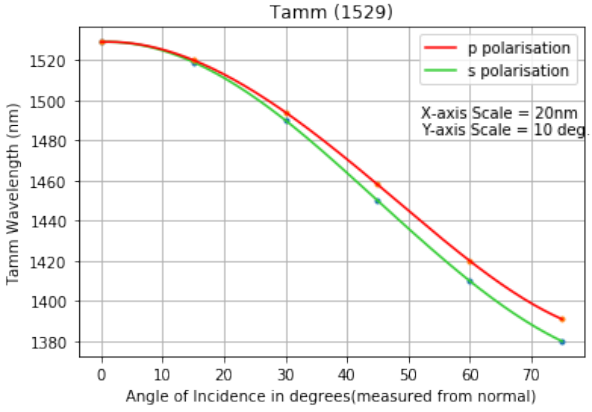

FIGURE 3.36: s and p Tamm wavelength vs Angle of Incidence 3

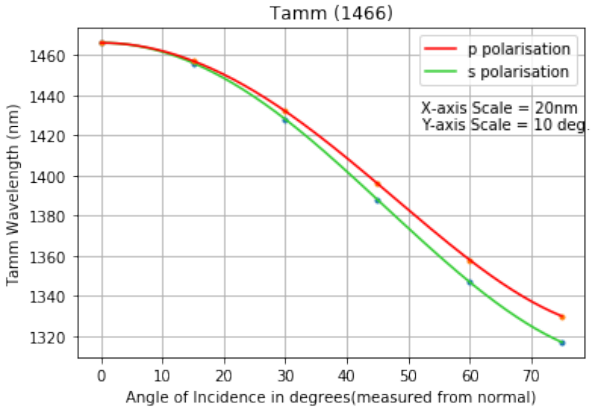

FIGURE 3.37: s and p Tamm wavelength vs Angle of Incidence 4

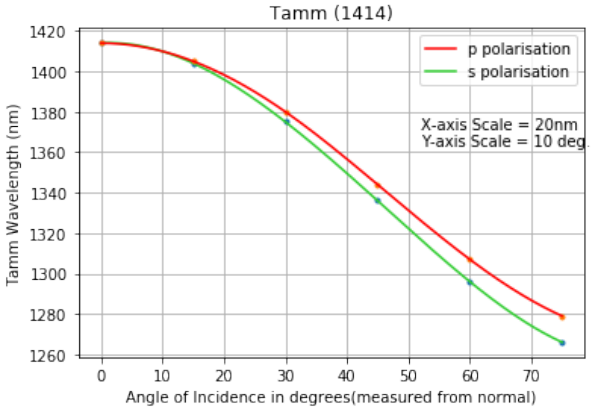

FIGURE 3.38: s and p Tamm wavelength vs Angle of Incidence 5

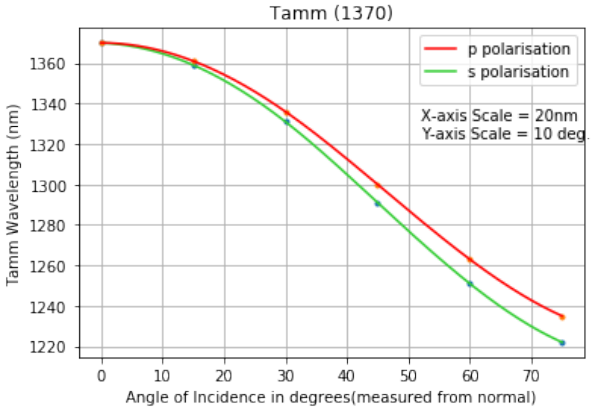

FIGURE 3.39: s and p Tamm wavelength vs Angle of Incidence 6

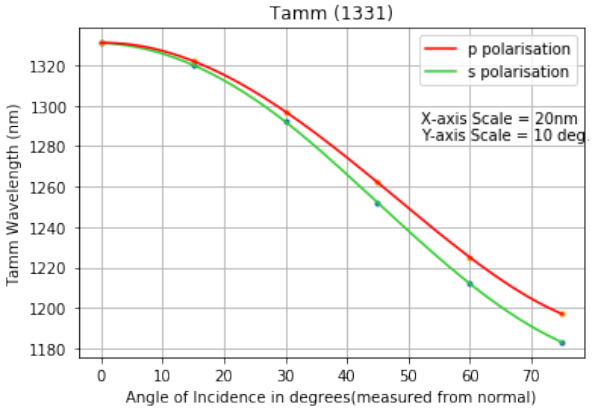

FIGURE 3.40: s and p Tamm wavelength vs Angle of Incidence 7

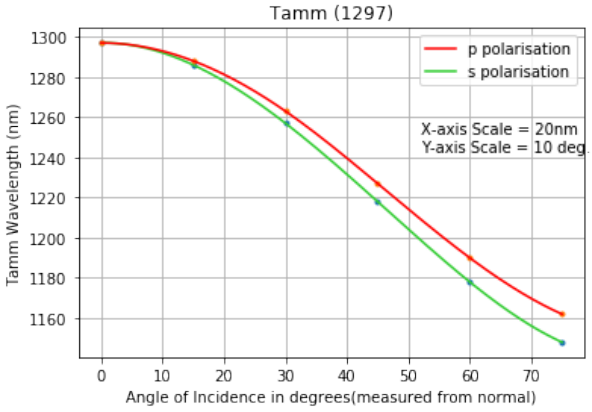

FIGURE 3.41: s and p Tamm wavelength vs Angle of Incidence 8

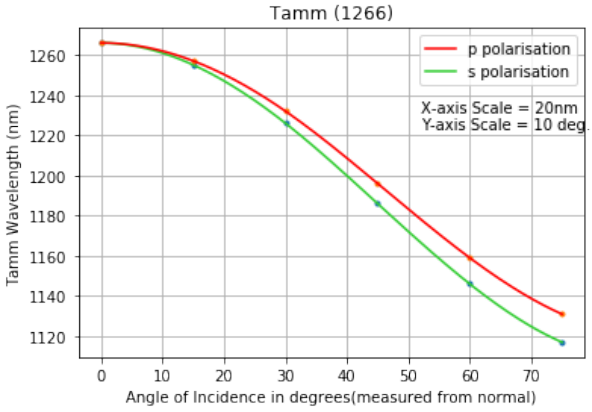

FIGURE 3.42: s and p Tamm wavelength vs Angle of Incidence 9

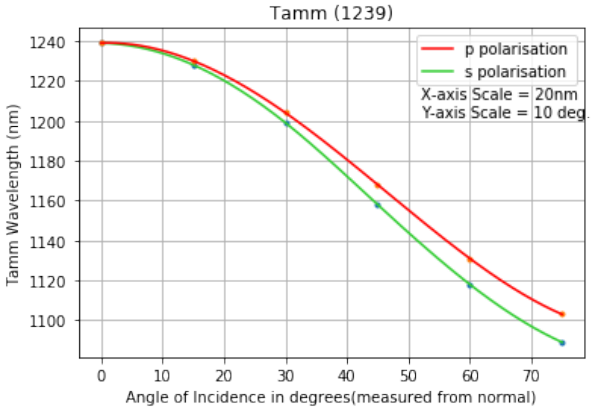

FIGURE 3.43: s and p Tamm wavelength vs Angle of Incidence 10

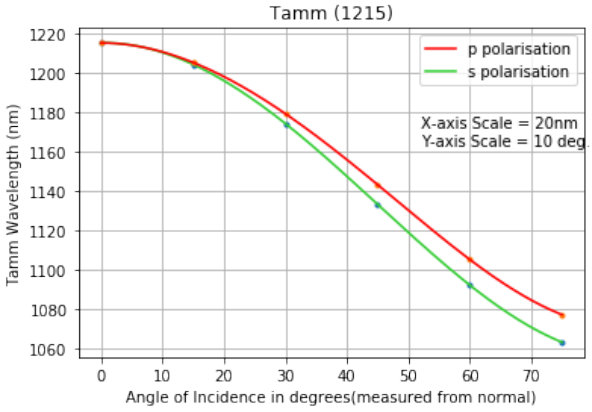

FIGURE 3.44: s and p Tamm wavelength vs Angle of Incidence 11

3.2.5 Change in difference between s and p polarised Tamm with angle variation

All of the Tamm modes(wavelengths) changed as the angle was varied for both polarisation. The difference between the Tamm wavelength of s polarised light and that of p polarised light is shown in the following table:

TABLE 3.13: Difference between s and p polarised Tamm with Angle variation

Incident Angle (in degrees)	Tamm 1 (1727 nm)	Tamm 2 (1610 nm)	Tamm 3 (1529 nm)	Tamm 4 (1466 nm)	Tamm 5 (1414 nm)	Tamm 6 (1370 nm)	Tamm 7 (1331 nm)	Tamm 8 (1297 nm)	Tamm 9 (1266 nm)	Tamm 10 (1239 nm)	Tamm 11 (1215 nm)
0	0	0	0	0	0	0	0	0	0	0	0
15	0	1	1	1	1	2	2	2	2	2	1
30	4	4	4	4	5	5	5	6	6	5	5
45	6	7	8	8	8	9	10	10	10	10	10
60	7	10	10	11	11	12	13	13	13	13	13
75	8	10	11	13	13	13	14	14	14	14	14

The plot of Angle vs The separation of s and p polarised Tamm wavelengths is plotted as below:

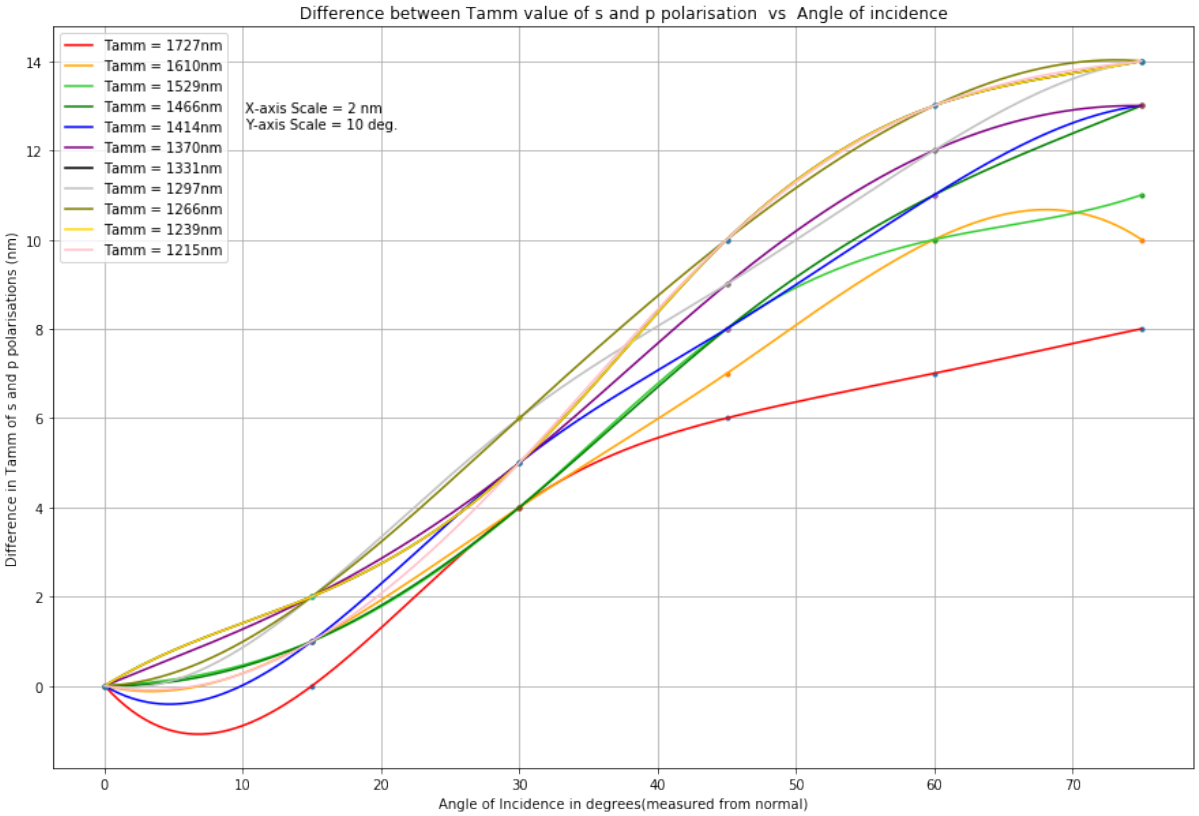

FIGURE 3.45: Angle vs The separation of s and p polarised Tamm wavelengths 1

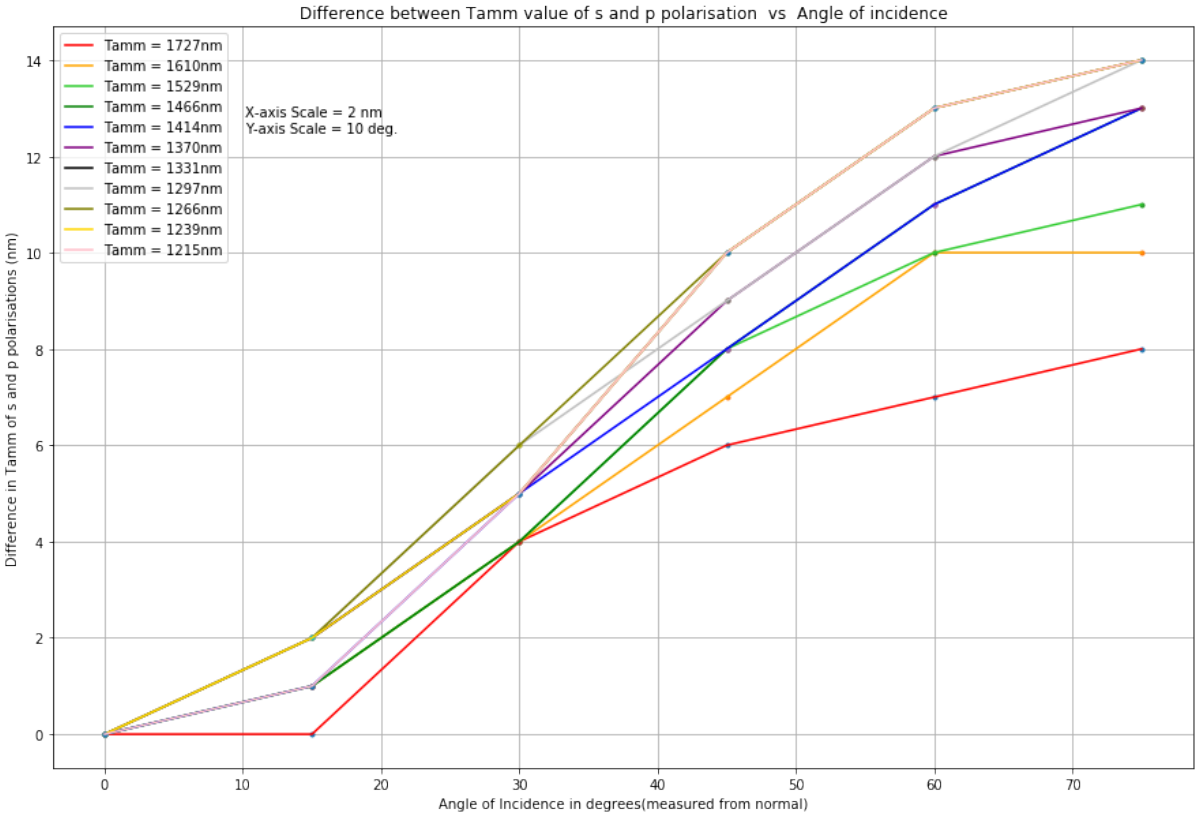

FIGURE 3.46: Angle vs The separation of s and p polarised Tamm wavelengths 2

Chapter 4

Discussions and Conclusion

4.1 Discussion on the Observations

4.1.1 Symmetric DBR

It can be observed that all the 20 cells in the DBR are identical and therefore it is a symmetric or periodic DBR. In subsection 3.1.1, several computationally simulated plots were obtained of the Reflectivity Spectrum for different incident angles. From figure 3.1 to 3.10 it can be observed that as the angle of incidence is increasing, the reflectivity is increasing and finally reaches 1 as the angle of incidence approaches 90 degrees, i.e. there is total reflection.
In each of the graphs, it is visible that there is only one Tamm mode for each band gap as the symmetry breaks only one time, i.e. due to the presence of the metal layer. And at the wavelength where Tamm is formed, there is a drop in Reflectance and no Transmittance is observed. In figure 3.11 it can be observed that the electric field intensity is really high just at the starting point and then, after that, there is no spike along x-axis, which confirms that there is no transmittance at Tamm wavelength. Therefore, absorption happens and standing waves are formed in between the metal and DBR.
Then, the shift in Tamm wavelength is observed for both polarisation s and p as the incident angle is changed and is plotted in figure 3.12, from where it can be seen that as the angle is increased, the separation between s and p is increased which occurs as the fresnel coefficients change for s and p differently. The Tamm that is being studied is the one in the band gap 1389 nm - 1904 nm.

4.1.2 Asymmetric DBR

In the asymmetric case, a DBR is constructed theoretically in which neither one of the cells is identical to another, in this DBR the width of one material keeps increasing while that of the other keeps decreasing in each successive cell.
In subsection 3.2.1, several computationally simulated plots were obtained of the Reflectivity Spectrum for different incident angles. Just like the Symmetric DBR case, from figure 3.13 to 3.22 it can be observed that the as the angle of incidence approaches 90 degrees, reflectance reaches 1. In the case of Asymmetric DBR, there are several Tamm modes in one band gap which occurs due to the breaking of symmetry many times in an Asymmetric DBR.
Here, 11 different Tamm wavelengths are the subject of study in the Band gap 1202 nm - 1923 nm. In figures 3.23 to 3.33 it can be seen that the Electric field intensity is maximum at different positions for different Tamm modes and there is a pattern that as the Tamm wavelength is increasing, the position at which the Intensity is maximum, is shifting forward. Also, just like the symmetric DBR, after the maximum intensity is reached, it drops suddenly and remains zero for the rest of the x axis, which again proves the fact that there is no transmittance at Tamm wavelength and that absorption occurs at this wavelength.
Now, from figure 3.34 to 3.44 the separation of s and p polarisation Tamm value change is plotted as the function of the angle change for all 11 different Tamm modes. Just like the symmetric DBR , in this case too, the separation between s and p increases as the angle increases for all Tamms.
After that, the separation between s and p for all Tamms was calculated and tabulated, from which, graphs 3.45 and 3.46 were plotted, in which the change of value of separation between s and p is studied for all Tamms and it can be deduced from the graphs and the Table that all Tamms follow same trend of increment of separation, however the matter of interest that can be seen is that the smaller wavelength the Tamm is, the faster the separation increases with increase in Incident angle, except the last two Tamms which are closer to one end of the Band gap.

4.2 Conclusion

From all of the above observations and discussions, we can conclude that the Asymmetric DBR mostly follows the same trend in Tamm modes as the symmetric DBR in theoretical simulations. However, the experimental part is still needed to be carried out in order to fully understand the concept of Tamm in different photonic crystal types.

REFERENCES

1. Charles Kittel. Introduction to Solid State Physics. John Wiley Sons, Inc., New York, 6th edition, 1986.

2. N.W. Ashcroft and N.D. Mermin. Solid State Physics. Saunders College, Philadelphia, 1976.

3. Steven G. Johnson. Introduction to photonic crystals : Bloch's theorem, band diagrams , and gaps (but no defects). 2003.

4. Aleksei P Vinogradov, Aleksandr V Dorofeenko, Aleksandr M Merzlikin, and Aleksandr A Lisyansky. Surface states in photonic crystals. Physics-Uspekhi, 53(3):243, 2010.

5. Alexander I. Lvovsky. Fresnel equations. In Taylor and Francis, editors, Encyclopedia of Optical Engineering, pages 1–6. Oxford University Press, Oxford, 2013.

6. S. J. Byrnes. Multilayer optical calculations. ArXiv e-prints, March 2016.

7. Yoel Fink. Lecture 23: Layered materials and photonic band diagrams. In Electronic, Optical and Magnetic Properties of Materials, Course No. 3.024. Cambridge MA, 2013. MIT OpenCourseWare.

8. Pochi Yeh, Amnon Yariv, and Chi-Shain Hong. Electromagnetic propagation in periodic stratified media. i. general theory. J. Opt. Soc. Am., 67(4):423–438, Apr 1977.

9. Tsz Kit Yung, Wensheng Gao, Ho Ming Leung, Qiuling Zhao, Xia Wang, and Wing Yim Tam. Measurement of reflection phase using thick-gap fabry–perot etalon. Appl. Opt., 55(26):7301–7306, Sep 2016.